Atmos. Chem. Phys., 14, 12683–12699, 2014
www.atmos-chem-phys.net/14/12683/2014/
doi:10.5194/acp-14-12683-2014

Atmospheric Chemistry and Physics
Open Access

Atmospheric black carbon and warming effects influenced by the source and absorption enhancement in central Europe

S. Nordmann[1,2], Y. F. Cheng[3,2], G. R. Carmichael[3], M. Yu[3], H. A. C. Denier van der Gon[4], Q. Zhang[5], P. E. Saide[3], U. Pöschl[2], H. Su[2], W. Birmili[1], and A. Wiedensohler[1]

[1]Leibniz-Institute for Tropospheric Research, Leipzig, Germany
[2]Multiphase Chemistry Department, Max Planck Institute for Chemistry, Mainz, Germany
[3]Center for Global and Regional Environmental Research, University of Iowa, Iowa City, IA, USA
[4]TNO Built Environment and Geosciences, Utrecht, the Netherlands
[5]Center for Earth System Science, Tsinghua University, Beijing, China

Correspondence to: S. Nordmann (stephan.nordmann@mpic.de)

Received: 14 April 2014 – Published in Atmos. Chem. Phys. Discuss.: 5 June 2014
Revised: 10 October 2014 – Accepted: 22 October 2014 – Published: 2 December 2014

Abstract. Particles containing black carbon (BC), a strong absorbing substance, exert a rather uncertain direct and indirect radiative forcing in the atmosphere. To investigate the mass concentration and absorption properties of BC particles over central Europe, the model WRF-Chem was used at a resolution of 12 km in conjunction with a high-resolution BC emission inventory (EUCAARI 42-Pan-European Carbonaceous Aerosol Inventory; 1/8° × 1/16°). The model simulation was evaluated using measurements of equivalent soot carbon, absorption coefficients and particle number concentrations at seven sites within the German Ultrafine Aerosol Network, PM_{10} mass concentrations from the dense measurement network of the German Federal Environmental Agency at 392 monitoring stations, and aerosol optical depth from MODIS and AERONET. A distinct time period (25 March to 10 April 2009) was chosen, during which the clean marine air mass prevailed in the first week and afterwards the polluted continental air mass mainly from the southeast dominated with elevated daily average BC concentration of up to 4 µg m^{-3}. The simulated PM_{10} mass concentration, aerosol number concentration and optical depth were in good agreement with the observations, while the modelled BC mass concentrations were found to be a factor of 2 lower than the observations. Together with back trajectories, detailed model bias analyses suggested that the current BC emission in countries to the east and south of Germany might be underestimated by a factor of 5, at least for the simulation period. Running the model with upscaled BC emissions in these regions led to a smaller model bias and a better correlation between model and measurement. In contrast, the particle absorption coefficient was positively biased by about 20 % even when the BC mass concentration was underestimated by around 50 %. This indicates that the internal mixture treatment of BC in the WRF-Chem optical calculation is unrealistic in our case, which overamplifies the light absorption by BC-containing particles. By adjusting the modelled mass absorption cross-section towards the measured values, the simulation of particle light absorption of BC was improved as well. Finally, the positive direct radiative forcing of BC particles at the top of the atmosphere was estimated to be in the range of 0 to +4 W m^{-2} over Germany for the model run with improved BC mass concentration and adjusted BC light absorption cross-section. This adjustment lowered the positive forcing of BC by up to 70 %, compared with the internal mixing treatment of BC in the model simulation.

1 Introduction

Black carbon (BC) particles are characterized by their ability to strongly absorb solar radiation across a broad spectrum of wavelengths (Bond and Bergstrom, 2006). Shortly after their emission from incomplete combustion, these particles have sizes around 100 nm (Rose et al., 2006), which may change during atmospheric transport due to ageing processes. The ageing alters the chemical composition, the microphysical

and optical properties of BC-containing particles. In the atmosphere, BC particles directly affect the climate by heating their environment or by changing the surface albedo, when deposited on snow. Upon emission from combustion sources, BC-containing particles are usually hydrophobic and unlikely to act as cloud condensation nuclei (CCN; Weingartner et al., 1997; Rose et al., 2011). But upon atmospheric ageing and mixing with water-soluble substances they can become hydrophilic and CCN-active (Khalizov et al., 2009; Spracklen et al., 2011). An example of the semi-direct effect of BC particles is their incorporation into cloud processes, which may reduce cloud lifetime and cover by heating and evaporating cloud droplets (Ackerman et al., 2000). On the other hand, when located below or above clouds, a BC-containing layer may enhance cloud cover by changing the local temperature field, which causes a negative semi-direct effect (Koch and Del Genio, 2010).

In the literature, there is much ambiguity in measurements and in models regarding the definition of soot (Petzold et al., 2013). The most common terms for this carbonaceous species are elemental carbon (EC) or BC – which are not necessarily the same, because measurements may be influenced by both BC mixing state and brown carbon (e.g. HULIS, tarry material from combustion) to a different extent (Andreae and Gelencser, 2006). However, BC and EC are often used interchangeably in modelling studies (Vignati et al., 2010). In this study, we will often use the term soot carbon (C_{soot}) according to the definition given in Andreae and Gelencser (2006), when referring to equivalent soot carbon measurements from Nordmann et al. (2013) for model evaluation. For simplicity and due to a lack of more rigorous alternatives, we assume in this study that the modelled BC concentrations are equivalent to the measured C_{soot} concentrations.

The Intergovernmental Panel on Climate Change (IPCC, 2013) reports a radiative forcing of 0.4 (0.05–0.8) Wm^{-2} for BC from the combustion of fossil fuel, 0.2 Wm^{-2} for BC from biomass burning and 0.04 (0.02–0.09) Wm^{-2} for BC deposited on snow. Current uncertainties in modelling the climate effect of BC on global and regional scales may be due to uncertainties in BC mass concentrations (e.g. uncertainties in emissions, as well as in model treatment of BC ageing and removal processes) and in the calculation method of its optical properties (Koch et al., 2009). Radiative transfer modules in regional and global models usually need the aerosol optical depth (AOD) and single scattering albedo (SSA) for considering aerosol optical properties in the calculation. A typical approach for deriving AOD in these models is the application of mass extinction cross-sections together with mass concentrations and hygroscopic growth factors of individual compounds (Kinne et al., 2006). BC is the major absorbing compound, for which mass absorption cross-sections have to be applied to derive the absorbing aerosol optical depth. Commonly used values of the mass absorption cross-section in different models show a large variation from 2.3 to 10.5 $m^2\,g^{-1}$ (Koch et al., 2009). The Weather Research and Forecast model coupled with a chemical transport module (WRF-Chem) uses a different approach by calculating the aerosol optical properties explicitly. For such purpose, Mie theory is applied using modelled volume size distributions in a sectional format. The advantage is that changes in the particle volume size distribution due to different chemical and physical processes in the atmosphere are taken into account when calculating the optical properties. However, the challenge is how to treat the BC mixing state in the Mie calculation (i.e. simplified by internal mixture, core-shell mixture or external mixture), which will significantly influence the calculated absorption (Bond and Bergstrom, 2006).

In this work, WRF-Chem is used in conjunction with a $1/8^\circ \times 1/16^\circ$ high resolution EC emission inventory (the EUCAARI 42-Pan-European Carbonaceous aerosol inventory) for estimating the concentration and radiative forcing of BC particles over central Europe, especially Germany. The model is evaluated using aerosol measurements from seven sites within the German Ultrafine Aerosol Network (GUAN) and PM_{10} mass concentrations on a daily basis from the dense measurement network of the German federal environmental agency (UBA) at 392 monitoring stations. A series of sensitivity studies of EC emissions are carried out in order to improve the simulation of BC mass concentration and to evaluate possible uncertainties in the sources. The model values of the mass absorption cross-section is first diagnosed from the model output and compared to the measurements from five sites within Germany, available for the simulated time period from Nordmann et al. (2013). Accordingly, the mass absorption cross-section is then adjusted in the model to further improve the simulations of soot light absorption and to estimate the radiative forcing of BC particles over Germany.

2 Methods

2.1 WRF – general model description

The Weather Research and Forecast model (WRF, version 3.2.1) is a state-of-the-art meteorology model (Skamarok et al., 2008), which is suitable for a broad spectrum of applications in simulating atmospheric phenomena of horizontal extents ranging from several hundred metres to thousands of kilometres (Grell et al., 2005). In WRF, the compressible and non-hydrostatic Euler equations are integrated to predict the wind, temperature, humidity and pressure fields, using the terrain-following hydrostatic pressure as the vertical coordinate. It can account for a variety of microphysical settings, ranging from simple bulk schemes to more sophisticated schemes allowing for mixed-phase cloud-resolving simulations. Planetary boundary layer physics are suitable for turbulent kinetic energy prediction. The surface may consist of several layers allowing for a vegetation and soil moisture

representation. The longwave and shortwave radiation field is calculated for a broad spectral region including clouds, gases and aerosol effects.

2.2 Aerosol representation

The emission, transport and ageing of aerosol particles is treated in the online coupled chemistry module, namely Chem. Online coupling allows for aerosol particles to directly influence the radiative transfer in the atmosphere. Moreover, they may act as CCN thereby changing the cloud cover and radiative effects of clouds. Clouds, in turn, may reduce aerosol concentrations by e.g. wet scavenging processes (Chapman et al., 2009).

For representing aerosol particles in WRF-Chem in this paper, the MOdel for Simulating Aerosol Interactions and Chemistry (MOSAIC) is used. In this model, aerosol particles are treated sectionally, which means that they are represented in a specific number of bins. Four bins are used in the present study, because of available calculation capabilities. With this model, mass and number concentrations of particles are simulated. MOSAIC treats the following chemical species: sulfate, methane sulfonate, nitrate, chloride, carbonate, ammonium, sodium, calcium, black carbon, organic carbon and other inorganic mass such as silica, other minerals and trace metals. For calculation of optical properties in the model, it is assumed that all compounds are internally mixed. Furthermore, particle growth and shrinkage may occur by an uptake of trace gases such as sulfuric acid, nitric acid, hydrogen chloride and ammonia. In addition particle coagulation and the formation of new particles by nucleation of sulfuric acid and water vapour are included (Fast et al., 2006; Zaveri et al., 2008).

In WRF-Chem, dry and wet deposition of aerosol particles are calculated. The scavenging of cloud-phase aerosol and below-cloud scavenging by interception and impaction are derived by using look-up tables. In addition, the dry deposition of aerosol in the lowest model layer is calculated by multiplying the concentrations with spatially and temporally varying deposition velocities. These velocities depend on the aerodynamic resistance, sublayer resistance and surface resistance (Grell et al., 2005). It is worth noticing that the particles are treated internally mixed in each bin, so theoretically, WRF-Chem tends to slightly overestimate the removal of BC, especially for the wet deposition processes. However, during our simulation period, there are mostly dry conditions in our domain.

2.2.1 Aerosol optical properties and radiative transfer in WRF-Chem

The method for calculating aerosol optical properties in WRF-Chem is described in detail in Barnard et al. (2010). Basically, an internal mixture of all chemical constituents is assumed for which the particle diameter and the refractive index are needed. The volume-equivalent particle diameter is derived by converting particle mass concentrations for each bin and each chemical compound into particle volume concentrations and afterwards dividing by the particle number concentration. The bulk refractive indices for each particle size bin are obtained by a mixing rule based on volume-weighted averaging. All these calculations are performed in the WRF-Chem subroutine called "optical_prep_sectional.F" in the module "optical_averaging.F". The aerosol particle optical properties, such as particle extinction and scattering cross-sections and asymmetry factor, are calculated online by a Mie code by the method described in Ghan et al. (2001). The optical module of WRF-CHEM was previously evaluated using measurements of the chemical composition as well as the particle light absorption and scattering coefficients in a measurement campaign, which took place in the Mexico City Metropolitan Area. Calculated values and observations of optical properties agreed within the limits of measurement uncertainty (Barnard et al., 2010).

The aerosol particle optical properties are calculated for four wavelengths (0.3, 0.4, 0.6 and 1 µm) and then passed to the Goddard radiation scheme (Chou et al., 1998). In this scheme, inter- and extrapolation is used to extend the wavelength range for the aerosol particle optical properties to 11 spectral bands between 0.18 and 10 µm. The transmission and reflection functions for each atmospheric layer are then calculated and a two-stream adding method is applied to derive the fluxes in the atmosphere and at the surface (Fast et al., 2006).

2.3 Model setup

2.3.1 Domains and settings

The model grid was chosen to consist of two nested domains with 27 vertical layers. The parent grid covers Europe with a spatial resolution of 36 km and is centred at 50.36° N and 16.07° E. The nested domain with a resolution of 12 km covers all of Germany and is shown in Fig.1. The time period from 23 March to 10 April 2009 was simulated, during which the general weather situation changed from more maritime- to more continental-influenced air masses.

The physics schemes used for simulation are summarized in Table 1. The microphysics scheme accounts for six forms of water including ice, snow and graupel. The surface physics include soil temperature and moisture in six layers. The boundary layer is represented by a prognostic turbulent kinetic energy scheme. Also included are schemes for surface physics, cumulus clouds and urban physics.

The model is driven by FNL[1] (final) operational global analysis data from NCEP (National Center for Environmental Prediction) on a 1.0°–1.0° grid, as meteorological boundary condition. The sea surface temperature is updated us-

[1] http://rda.ucar.edu/datasets/ds083.2/

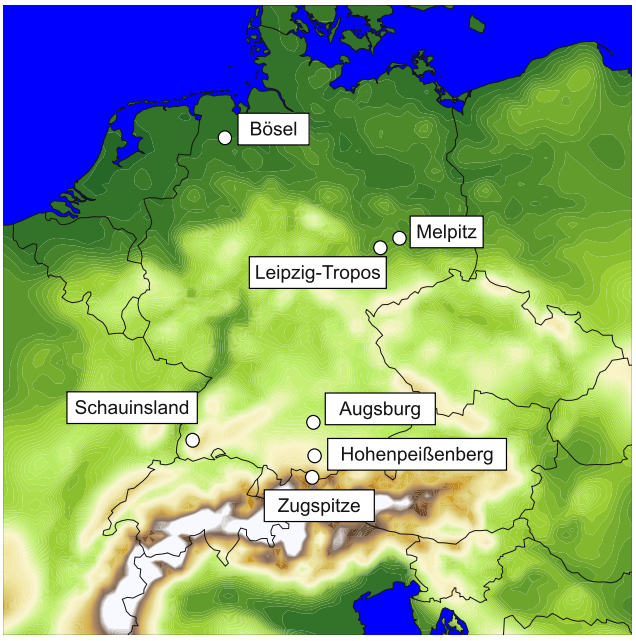

Figure 1. Locations of observation sites of C_{soot} mass concentration and light absorption in model domain D02 for model evaluation.

ing global satellite data from NCEP[2]. The information about the underlying surface including static fields of e.g. vegetation, terrain height and reflectivity are also taken into account by using the high-resolution data distributed with the WRF package.

2.3.2 Emissions

We used two different emission inventories, which largely differ in the horizontal resolution. The Pan-European Carbonaceous aerosol inventory for EC (Visschedijk and Denier van der Gon, 2008), which was developed in the framework of the EUCAARI (European Integrated project on Aerosol Cloud Climate and Air Quality interactions) project (Kulmala et al., 2011) for the year 2005 and is originally available on a $1/8° \times 1/16°$ longitude–latitude grid, corresponding to a resolution of around 7 km. For mapping the emissions on the model domains, it was assumed that they are equally distributed over all days of the year, applying only a diurnal variation. The assumed diurnal variation has two maxima. The first maximum is around 7 a.m. and the second maximum is around 5 p.m. The lowest emissions are around 2 a.m. The second inventory was developed in the Arctic Research of the Composition of the Troposphere from Aircraft and Satellites project (ARCTAS) and is available on a $1° \times 1°$ grid for the year 2008. EC emissions from EUCAARI are shown in Fig. 2. Because of the higher spatial resolution of the EUCAARI inventory, these EC emissions were mainly used in the present study. The EUCAARI inventory provides EC emissions but as EC and absorption-related BC are highly correlated (Nordmann et al., 2013), we use the EUCAARI EC inventory as the best approximation of BC emissions. Uncertainties in the emissions data will be explored later in the paper.

Table 1. Summary of physical settings.

Physics	Scheme
Microphysics	Lin et al. (1983)
Surface	Rapid Update Cycle (RUC) land surface model
Boundary layer	Mellor–Yamada–Janjic (Janjic, 1994)
Cumulus	Grell 3-D
Urban	1-layer urban canopy model
Shortwave radiation	Goddard scheme (Chou et al., 1998)
Longwave radiation	Rapid Radiative Transfer Model (RRTM)

We also compared the EUCAARI emissions to the Lamarque et al. (2010) data, taken from http://www.iiasa.ac.at/web-apps/tnt/RcpDb for the year 2005. In this inventory, the BC emissions were derived from Bond et al. (2007) and Junker and Liousse (2008). In Table S1, country-specific total emission numbers are shown for the EUCAARI and the Lamarque et al. (2010) inventory. This comparison indicates that the EUCAARI emissions are around 30 % higher in eastern European countries Poland, Czech Republic and Belarus.

Other emissions over Europe such as total PM, SO_2, NO_x, CO, NH_3 and NH_4 are used for the original $0.5° \times 0.5°$ grid and are taken from the European Monitoring and Evaluation Programme (EMEP). The emissions of volatile organic compounds (VOC) are given as total emissions from EMEP and were partitioned to compounds used in CBMZ chemical mechanism of WRF-Chem.

Biogenic emissions are taken from the model of emissions of gases and aerosols from nature (MEGAN) (Guenther et al., 2006). The Quick Fire Emission Dataset (QFED) biomass burning emissions were used in this study, in which the radiative power and location of fires is derived from the moderate resolution imaging spectroradiometer (MODIS) active fire product and combined with a vegetation classification data set (Darmenov and da Silva, 2013). The Finn utility (Wiedinmyer et al., 2011) was used to map the fire product to the model domains.

2.4 Observations

Measurements of meteorological variables, aerosol particles and gases are used for model evaluation. In a first step, the model is evaluated in terms of wind speed and direction, temperature and relative humidity using atmospheric sounding data[3].

For the evaluation of the WRF-Chem simulations of aerosol particles, data of the German Ultrafine Aerosol Net-

[2]http://polar.ncep.noaa.gov/sst/oper/Welcome.html

[3]http://www.weather.uwyo.edu/upperair/sounding.html

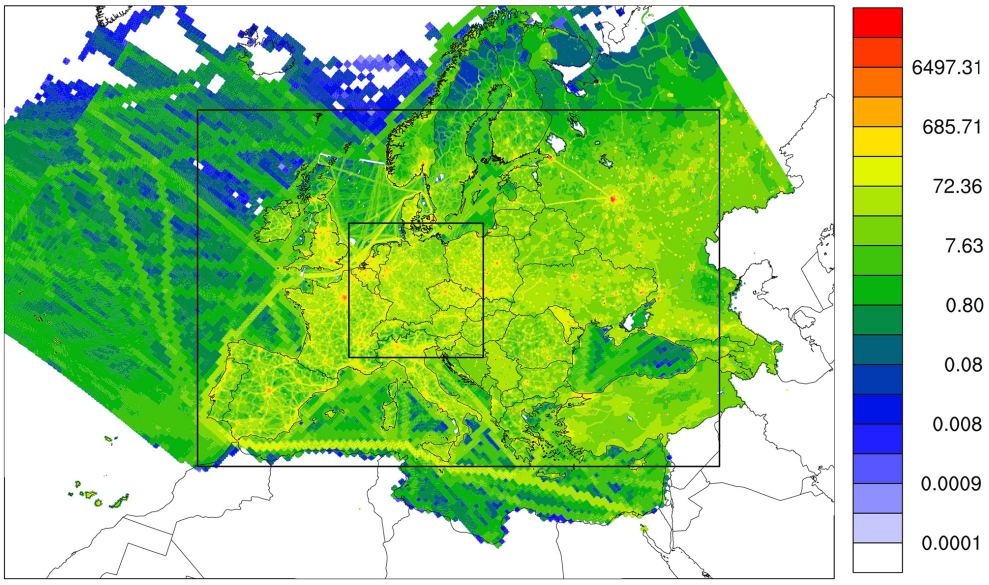

Figure 2. Emission rates of EC (kg m^{-2} yr^{-1}) from EUCAARI (resolution 7 km). The two nested model domains are indicated by black lines.

Table 2. Overview of the model runs, regarding EC emission inventory and calculation of absorption (setting of the BC refractive index).

Model run	BC emissions	Absorption settings	Emission totals in D01 (tons day^{-1})
R1	EUCAARI	0.71	0.65
R2	EUCAARI scaled to ARCTAS	0.26	0.62
R3	EUCAARI scaled by a factor of 2	0.26	1.30
R4	EUCAARI scales by a factor of 5 to the east of 15° E longitude	0.26	2.07
R5	EUCAARI set to 0	0.71	0

work (GUAN; Birmili et al., 2009) are used. The particle light absorption coefficient (σ_{ap}) is measured by multi-angle absorption photometers (MAAP; Petzold and Schönlinner, 2004), which are in excellent agreement with other particle light absorption photometers such as a photoacoustic sensor (Müller et al., 2011; Sheridan et al., 2005). Particle number size distributions in the submicrometre size range were measured in the GUAN network using mobility particle size spectrometers such as SMPS or DMPS.

In the MAAP instrument, particles are continuously sampled on filter tape, with loaded spots subsequently analysed by Raman spectroscopy to derive the particle mass concentration of C_{soot} (m_{Csoot}) (Nordmann et al., 2013). The cut-off sizes of the different MAAP instruments varied between 1 and 10 µm. The particulate C_{soot} mass concentrations were used to evaluate the model concerning simulated BC mass concentrations (m_{BC}) under the basic assumption that both are equivalent. Since C_{soot} mass concentrations are independent of the ageing process it is well suited for the comparison with model values of BC. In Nordmann et al. (2013) particle mass absorption cross-sections were determined from the combined MAAP–Raman method, which will be used to adjust the simulated aerosol absorption behaviour to real measurements.

PM_{10} mass concentrations on a daily basis from the dense measurement network of the German federal environmental agency (UBA) are compared to corresponding model values. Data of 392 sites with various characteristics from traffic to regional background related sites were considered. The simulation of gas concentrations of CO is compared with the measurements from the UBA network.

The vertical aerosol column is evaluated by using measurements of the aerosol optical depth (AOD) MODIS (Levy et al., 2007). In addition to the conventional Level 2 product, data with more restrictive filtering and bias correction with respect to AERONET according to Hyer et al. (2011) were used. Sun photometer measurements from the aerosol robotic network (AERONET, Holben et al. (1998)) were also applied for a rough quality check of the MODIS data.

3 Results and discussion

3.1 Source evaluation

In this section, the model evaluation concerning aerosol particle microphysical and optical properties is presented. The evaluation of the modelled meteorology for the model base run (R1, see Table 2) was done by using atmospheric sounding data of nine stations in Germany. In principle, the model simulates the meteorology well with a small negative bias in temperature and a small positive bias in wind speed and relative humidity. All evaluation results for R1 are summarized in Table 3.

3.1.1 BC mass concentration

The modelled BC mass concentrations were compared to C_{soot} mass concentrations measured by Raman spectroscopy as described in Nordmann et al. (2013). Measured particle mass concentrations were available on a daily basis. The mean normalized bias (MNB) and R^2 at all observation sites are summarized in Table 4. As an example, the time series at the regional observation site Bösel and corresponding model values are shown in Fig. 3a for the model run R1 (R3 and R4 refer to additional model runs with scaled emissions as described later in detail in Sect. 3.1.5 and Table 2). At Bösel site, the measured m_{Csoot} increased from around 0.5 to a maximum of about 1.5 µg m^{-3} during this time period. A similar trend can also be seen in the modelled m_{BC} in the base run R1, but on a lower level. The correlation between model and observation (R^2) is 0.61 and MNB is −21 % (Table 4). At the urban background site Leipzig-TROPOS, the modelled m_{BC} is about 70 % lower than the observation and the correlation is $R^2 = 0.35$. At the higher-altitude sites, the modelled m_{BC} again also correlates well with measurements, for example with R^2 of 0.66 at mid-level mountain site Mt Hohenpeißenberg and R^2 of 0.79 at the Alpine mountain site Zugspitze, but the modelled m_{BC} is also negatively biased with MNB between −50 % and −80 %. Calculating the overall deviation of the model, m_{BC} is about 0.71 µg m^{-3} too low, which corresponds to MNB of −53 % as can be seen in Table 4. Genberg et al. (2013) found a 69 % underestimation of BC for the regional site Melpitz and attributed this to an emission underestimation in the southwest, according to the main wind direction.

Although there was a significant amount of biomass burning activities in the Ukraine and parts of Russia in the second half of the simulation period, the influence on the BC mass concentration at the observation sites in Germany is very small (Fig. S1). This indicates that biomass burning activities cannot be responsible for the overall large bias found for the BC mass concentrations.

In Fig. 4 the 72 h back trajectories coloured according to the MNB values are shown. Especially in the southern and the eastern part of Germany several trajectories indicate that air masses arrived from continental origins to the east of Germany. As described in Nordmann et al. (2013) this was mainly the case in the second half of the simulation period. However, the trajectories indicate that the negative model bias is increased for continental air masses. In order to evaluate whether the underestimation of BC concentration is mainly due to uncertainties in the model or in the emission sources, we will compare other modelled aerosol and gas phase species with observations in the following sections, e.g. aerosol mass and number concentration, aerosol optical depth and CO.

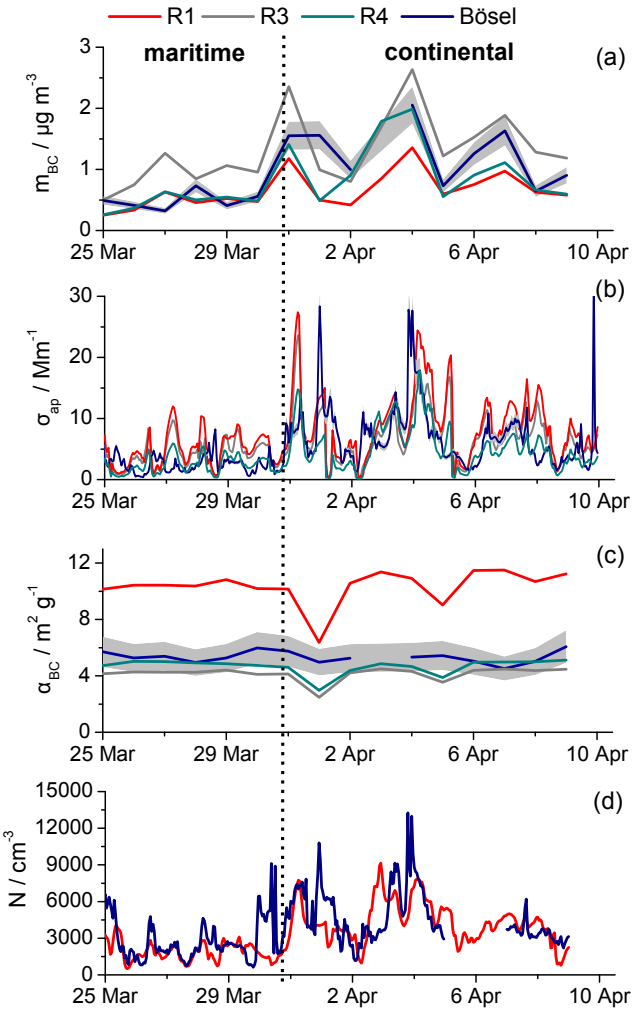

Figure 3. Comparison between measured C_{soot} and modelled BC mass concentrations (m_{BC}) **(a)**, absorption coefficient (σ_{ap}) **(b)**, mass absorption cross-sections (α_{BC}) **(c)** and particle number concentration (N) **(d)** at the regional observation site Bösel. Besides the results for model base run R1, the time series from additional model runs R3 and R4 are also shown, which differ from R1 in the EC emissions and the calculation of optical properties (see Table 2).

Table 3. Summary of values of mean bias (MB), mean normalized bias (MNB), root mean square error (RMSE) and coefficient of determination (R^2) derived from a comparison of different measurements and corresponding model values simulated in R1. The PM_{10} statistics refer to the maritime/continental split of the simulation period. The AOD statistics refer to the sunphotometer observation technique. The results of the model meteorology comparison are shown for the surface layer as an average over the simulation period.

Class	Model variable	Number of sites	MB	MNB	RMSE	R^2
Meteorology	T (°C)	9	−1.27	−0.06	2.39	0.98
	u (ms^{-1})	9	0.16	0.37	2.92	0.92
	v (ms^{-1})	9	0.13	0.32	2.84	0.90
	RH (%)	9	4.83	0.60	17.81	0.72
Gas	CO (ppmv)	2	−0.10	−0.61	0.11	0.36
Aerosol	PM_{10} ($\mu g\,m^{-3}$)	392	−2.51/−9.73	−0.04/−0.14	9.10/18.69	0.25/0.41
	BC ($\mu g\,m^{-3}$)	5	−0.71	−0.53	1.07	0.35
	Number (m^{-3})	8	−3.50	0.34	6.03×10^{-6}	0.16
Aerosol optics	AOD	2	-0.02	-0.04	0.03	0.61
	$\sigma_{ap\text{-}wet}$ (Mm^{-1})	7	−1.07	0.34	37.63	0.17
	$\sigma_{ap\text{-}dry}$ (Mm^{-1})	7	−1.57	0.20	36.73	0.18
	$\alpha_{BC\text{-}wet}$ ($m^2\,g^{-1}$)	5	6.42	1.33	42.54	0.01
	$\alpha_{BC\text{-}dry}$ ($m^2\,g^{-1}$)	5	5.34	1.11	30.35	0.01

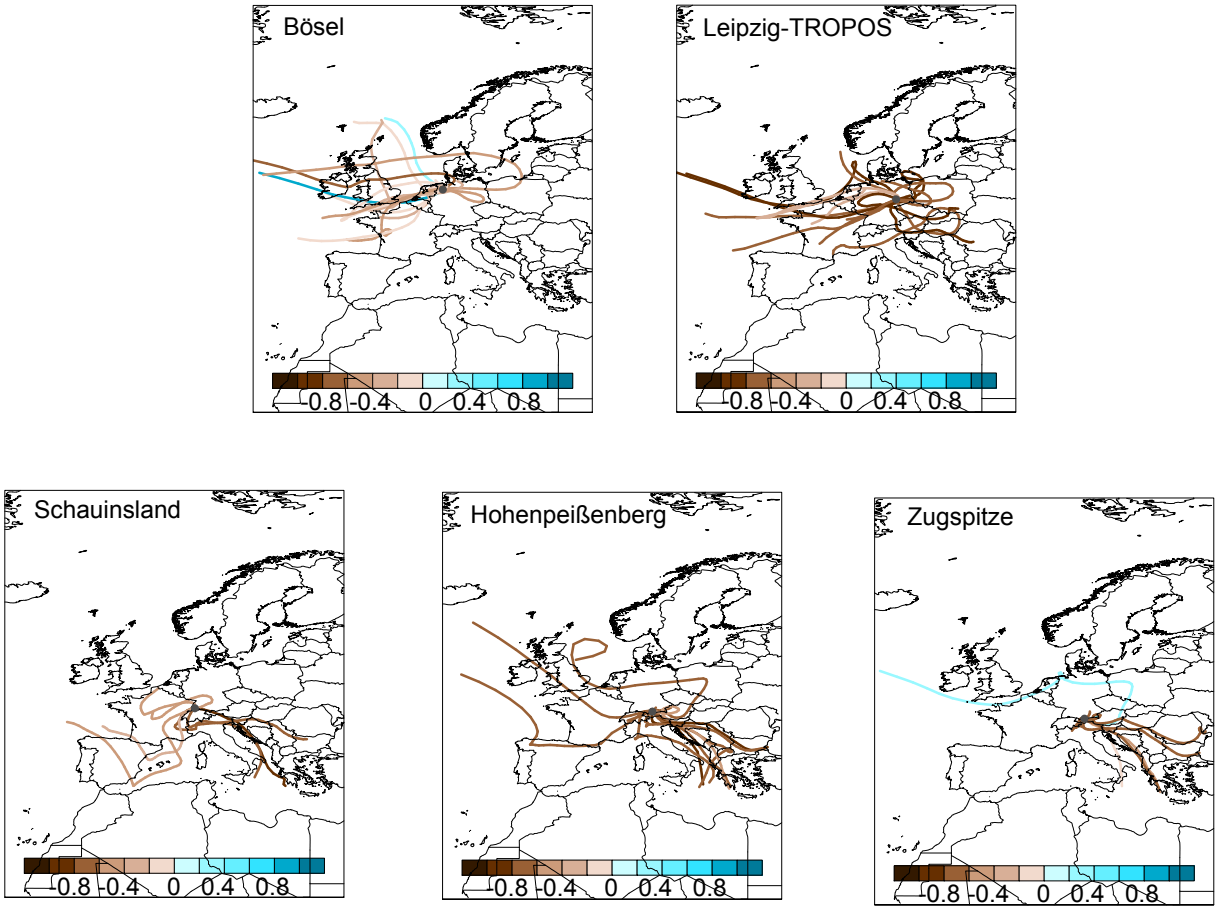

Figure 4. 72 h back trajectories calculated from the model output (D01) for different observation sites in the GUAN network. The trajectories are coloured according to the MNB for individual observation sites.

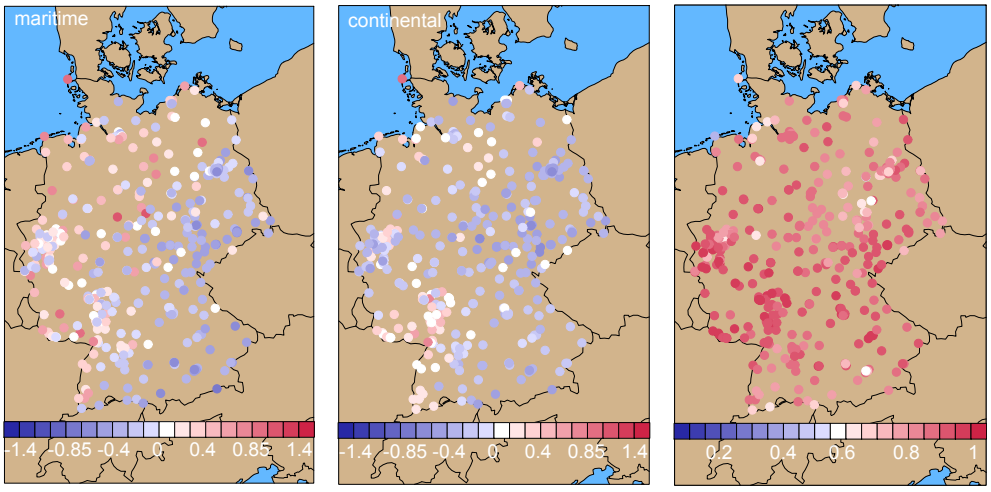

Figure 5. Comparison between modelled and measured daily PM_{10} mass concentrations for the more maritime time period (24 March–31 March 2009) and the more continental time period (1 April–9 April 2009) in terms of the mean normalized bias (MNB) is shown. The right figure depicts the correlation coefficient. Measurements performed by the German Federal Environmental Agency (UBA).

3.1.2 Aerosol mass and number concentrations

The simulated PM_{10} mass concentrations from the base run R1 were compared to UBA measurements. For this purpose, the daily averaged PM_{10} mass concentrations were considered. The results of this comparison in terms of MNB are shown for the more maritime and more continental time periods in Fig. 5. Among the 392 monitoring stations over Germany, the overall correlation between modelled and observed PM10 is quite good with R^2 of 0.60. Compared to the BC simulation, the model bias in PM_{10} is much smaller with an overall average MNB of about −9 %. However, we could still clearly see the pattern that the model slightly overestimates the PM_{10} mass in the western part and underestimates in the eastern part of Germany. The overprediction of PM_{10} by the model, especially in the maritime air mass and for locations not far away from the sea, may be attributed to an overestimation of the sea salt emission calculated in the WRF-Chem. Zhang et al. (2013) also found an overestimation of PM_{10} for several European observation sites and attributed this to an overestimation of the sea salt emission by WRF-Chem. The underestimation is especially true for the continental time period during which the average MNB is about −14%, while it is only about −4 % during the marine time period.

The total aerosol number concentration from mobility particle size spectrometer measurements with a temporal resolution of 1 h in GUAN was compared to model values. The modelled values in the first three Mosaic bins were summed in order to match the measured particle sizes (<1 µm). The time series for a regional observation site is shown in Fig. 3d. In general, the modelled total aerosol number concentration follows the trend of the observations. Taking all observation sites into account, a positive MNB of 34 % was derived (see Table 3), with the best correlation for the comparison with regional observation sites, for example R^2 = 0.27 at Bösel.

3.1.3 Aerosol optical depth

The aerosol optical depth (AOD) is defined as the particle-induced light extinction along a specific path. Therefore, an AOD comparison between model and measurement gives some evidence about how well the model simulates the vertical distribution of aerosol particles.

Because WRF-Chem calculates aerosol particle optical properties only for four wavelengths, linear interpolation between AOD at 400 and at 600 nm was used to derive the AOD at 550 nm. The WRF data were masked according to the availability of MODIS data. The average MODIS AOD in the modelling period ranged between 0.05 and 0.6. The model simulated a broader range with 0.01 to 0.8. In Fig. 6, the horizontal distribution of MNB is shown. Over most regions in central Germany there is a negative model bias around −40 % for the Level 2 MODIS products (left panel in Fig. 6). On the other hand, especially in the southwestern and northeastern part, the model overestimates AOD up to 200 % for the Level 2 MODIS AOD (left panel in Fig. 6). However, when additional filtering processes were applied to the MODIS AOD data following Hyer et al. (2011), the model bias in this region become significantly smaller (right panel in Fig. 6). A possible explanation for the overestimation of AOD in the southwestern part of Germany may be the lack of detailed information of the stack height of point source emissions. This may lead to an underestimation of pollutant emissions to higher atmospheric levels in this densely populated region. On the other hand, the overestimation in the northeastern part may be attributed to overestimated sea salt concentrations in lower atmospheric levels as previously

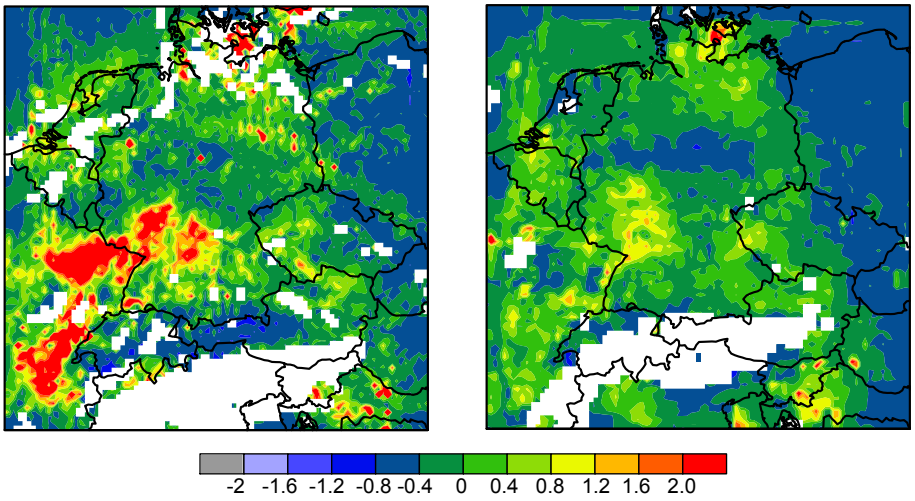

Figure 6. Mean normalized bias in AOD (dimensionless) from comparison with MODIS measurements. Two different products were used, Level 2 (left) and data with additional quality assurance filters according to Hyer et al., 2011 (right). Simulated values of AOD were considered for times and locations with available MODIS data.

mentioned for the PM_{10} model comparison. Contrastingly, the largest negative model bias in domain 2 can be seen over the large area of Poland and the Czech Republic (right panel in Fig. 6). It also extends to most of the regions in the countries to the east of Germany. This implies that the emissions are underestimated in the eastern part of the modelling domain.

At least, it has to be pointed out that the uncertainties in the AOD itself may also contribute to these discrepancies in the comparison. In previous studies, the MODIS AOD product was evaluated with AERONET sun photometer measurements and it was found that MODIS AOD is often positively biased by up to 50 % (Schaap et al., 2008) and 48 % (Remer et al., 2005) over the European land surface. This bias was attributed to uncertainties in land surface reflectance in the MODIS AOD retrieval and possible cloud contamination (Schaap et al., 2008). Considering these findings, we also compared the simulated AOD to AERONET sunphotometer measurements performed at two observation sites in Germany (Fig. 7). Regarding only the AOD of those two AERONET sites, the model follows nicely the measured AOD ($R^2 = 0.61$) and the MNB was found to be only -4 % (see Table 3). Consequently, if the 50 % positive bias of the MODIS AOD in comparison to the "true AOD" (AERONET AOD) is considered, our model results are actually closer to the "true values", indicating a general good model performance in the simulation of AOD.

3.1.4 Carbon monoxide

Because of the large negative bias found for the simulation of m_{BC}, the model performance of CO, as the most related gas phase species to the combustion process, was also checked. The volume mixing ratios of CO from hourly measurements at three observation sites of the UBA network were compared to the corresponding model values from the base run R1. At both, the regional and the mountain observation site, the CO concentrations show a similar temporal behaviour with an overall R^2 of 0.36. A substantial negative bias of 61 % was calculated, which is very similar to the bias found for m_{BC}, therefore suggesting that emissions from combustion processes may be significantly underestimated.

3.1.5 BC source adjustment

As discussed before, the modelled BC mass concentrations were found generally too low in comparison to the ground-based measurements. Trajectory analysis of the model bias indicates that the largest model bias in the BC mass concentration was found when the air masses came from the eastern and southeastern directions. Considering that the meteorology was well simulated by the model and taking also the results for PM_{10} and AOD into account, there are strong indications that emission rates in regions to the east of Germany may be underestimated for the period evaluated.

To verify the assumption of underestimated EC emissions, three additional model runs were performed in order to improve the simulation of BC mass concentrations, as summarized in Table 2. For the second model run (R2), the EUCAARI EC emissions were spatially scaled to the ARCTAS BC inventory level to account for possible emission changes from 2005 to 2008. The scaling was done by calculating the EC emissions in both inventories on a $1^\circ \times 1^\circ$ grid. Dividing each ARCTAS emission rate in individual 1° grid cell by the corresponding EUCAARI EC emission rate in the same grid cell, a scaling map was derived. This scaling map was then applied on the original EUCAARI emission inventory to conserve its high spatial resolution. The scaling leads to

Table 4. Site-dependent statistical evaluation of model simulation of BC mass concentration and absorption coefficient in terms of mean bias (MB), mean normalized bias (MNB), root mean square error (RMSE) and coefficient of determination (R^2).

Site	location	BC mass concentration				Absorption coefficient			
		MB	MNB	RMSE	R^2	MB	MNB	RMSE	R^2
Augsburg	48.36° N, 10.91° E					−6.69	−0.52	11.09	0.13
Leipzig-TROPOS	51.35° N, 12.43° E	−1.57	−0.70	1.82	0.35	−3.30	−0.12	7.67	0.18
Melpitz	51.54° N, 12.93° E					−0.59	0.31	4.23	0.41
Bösel	53.00° N, 7.96° E	−0.31	−0.21	0.46	0.61	1.93	1.07	5.12	0.27
Hohenpeißenberg	47.80° N, 11.00° E	−0.59	−0.72	0.72	0.66	−1.54	−0.26	2.57	0.42
Schauinsland*	47.91° N, 7.91° E	−0.87	-0.55	1.05	0.01	1.00	0.51	3.47	0.04
Zugspitze	47.42° N, 10.98° E	−0.26	−0.46	0.37	0.79	−0.46	0.58	1.24	0.59

* Measurements are not available for the whole simulation period.

an increase of emissions especially in the western and southwestern part of Germany and in Poland (Fig. S2). However, it is worth noticing that different methodologies were used for developing both inventories, which may also result in differences in emission numbers. This scaling procedure results in a slightly lower total emission rate in the modelling domain of 0.62 tons day^{-1} in comparison to the emission from the original EUCAARI inventory (Table 2). For model run R3, the EUCAARI EC emissions were simply multiplied by a factor of 2, which is justified by the fact that global BC emission estimates may vary by a factor of 0.5–2 (Vignati et al., 2010). For model run R4, another scaling procedure was applied, in which the inventory was scaled by a factor of 5 but only for locations to the east of 15° E longitude. This scaling strategy is supported by the fact that the BC model bias is higher when the continental air masses were originated from the east and southeast. It is also justified by the fact that the BC emission may vary by a factor of 2–5 on a regional scale (Ramanathan and Carmichael, 2008). On a related note, Chi et al. (2013) also reported that by using EMEP CO emissions in a simple Lagrange disperse model, the simulated CO concentration was by a factor of 5 lower than the observation at a remote boreal forest site in Russia. This scaling method increases the total emission in the domain to 2.07 tons day^{-1}. For R5 in Table 2 the EC emissions are set to 0 for calculating the radiative forcing, which will be described later.

In general, an increase of simulated m_{BC} towards the measured values can be seen for the three additional model runs (Table 5). The simulation of BC is improved with MNB −36 % for R2, −6 % for R3 and −40 % for R4. The simulation of the temporal pattern remains nearly unchanged for R2 ($R^2 = 0.35$) and R3 ($R^2 = 0.37$). This is because although the overall model bias improved significantly in R3, as shown in Fig. 3, the modelled value matches the observation during the polluted continental time period, while the simulations during the clean marine time period degraded with pronounced overestimation by a factor of 2. This indicates that during the clean marine time period the EC emissions in Germany and in the countries to the west are not necessarily underestimated. However, the run R4 improved the correlation between model and observation to $R^2 = 0.45$, which captures the observed temporal pattern during both marine and continental polluted periods. For 1–2 April and 6–7 April 2009, the BC mass concentration is still underestimated by R4. This may be due to slight underestimation of EC emissions to the west of 15° E or the emissions to the east of 15° E being underestimated by more than a factor of 5.

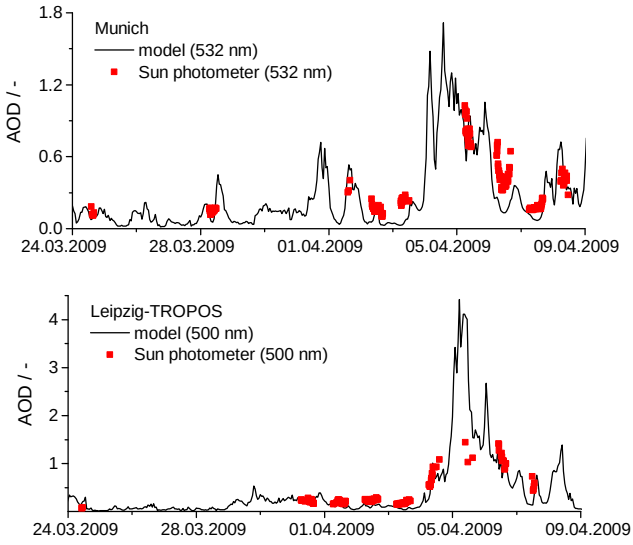

Figure 7. Time series of AOD from AERONET sun photometer measurements with model values shown as straight lines.

It is worth noticing that there might also be interannual/monthly variation in the EC emission, which we kept constant. However, if monthly variation were taken into account, spring time (April) would be the relatively lower emission time period in comparison to the heating time period in winter. This means that we actually already have an overfeed in emission into the model run. It further justifies that the annual emission of BC that we are using now is even more strongly underestimated.

Table 5. Summary of values of mean bias (MB), mean normalized bias (MNB), root mean square error (RMSE) and coefficient of determination (R^2) derived from a comparison of different measurements and corresponding model values simulated in the runs R2, R3 and R4.

Class	Model variable	Number of sites	Run	MB	MNB	RMSE	R^2
Aerosol	PM_{10} ($\mu g\,m^{-3}$)	392	R2	−2.40	−0.07	13.71	0.59
			R3	−5.30	−0.06	14.24	0.61
			R4	−5.77	−0.08	14.37	0.61
	BC ($\mu g\,m^{-3}$)	5	R2	−0.56	−0.36	0.83	0.35
			R3	−0.30	−0.06	0.54	0.37
			R4	−0.55	−0.4	0.73	0.45
Aerosol optics	$\sigma_{ap\text{-}dry}$ (Mm^{-1})	7	R2	−3.23	−0.23	40.89	0.22
			R3	−2.51	−0.04	38.61	0.20
			R4	−3.31	−0.33	42.54	0.20
	$\alpha_{BC\text{-}dry}$ ($m^2\,g^{-1}$)	5	R2	−0.15	−0.01	0.58	0.00
			R3	−0.87	0.16	1.39	0.00
			R4	−0.44	−0.07	0.76	0.00

3.2 Evaluation of particle light absorption and warming effects

3.2.1 Evaluation of particle light absorption

Aerosol particle optical properties such as the particle light extinction coefficient, single scattering albedo and asymmetry factor are determined in WRF using Mie theory as described before. Using output variables of the particle light extinction coefficient and single scattering albedo at wavelengths of 600 and 1000 nm, the particle light absorption coefficient at the MAAP wavelength of 637 nm can be derived from the model output by linear interpolation. All measurements were performed for dry aerosol particles, which is a problem when comparing with the modelled light absorption coefficient, because simulated values are derived for particles at ambient conditions. In several studies, it was shown that BC, internally mixed with hydrophilic substances (e.g. sulfate) is able to take up water, which then amplifies the absorption of solar radiation (Fuller et al., 1999; Nessler et al., 2005; Mikhailov et al., 2006). For that reason, the particle optical properties were calculated again, after the model run was finished, using an offline version of the module "optical_averaging.F" in WRF-Chem and the simulated concentrations of the chemical constituents. For this offline run of the optical module, the aerosol water content was removed.

In Fig. 3b, the modelled and measured hourly values of the dry absorption coefficients are shown for one regional observation site. Corresponding statistics are shown in Table 4. An increase of σ_{ap} occurred in association with an increase in BC mass concentration in the continental air mass. For the base case model run R1, regarding the urban sites, the increase is clearly visible in model values, at least for Leipzig-TROPOS. The model underestimates σ_{ap}, especially for the station in Augsburg. MNB at urban sites is between −12 % and −52 % with values of R^2 between 0.13 and 0.18. At the regional sites, the model simulates the absorption coefficient better, so that even some peak values are reflected in the model output. In addition, the correlation is better than at urban sites with values of R^2 between 0.27 and 0.41, but in the entire period the model is positively biased with MNB between 31 % and 107 %. At the mid-level mountain sites the model is again on the level of measured σ_{ap}, except for some shorter time periods at the beginning of April at Mt Hohenpeißenberg. The values of MNB are between −26 % and 51 % with coefficients of determination between 0.04 and 0.42. For the observation site Schauinsland, only data from the continental air mass were available. The best correlation between model and measurement is found for the Alpine mountain site Zugspitze, with $R^2 = 0.59$ and a positive bias around 58 %. In summary, a value of MNB = 20 % was found as an average over all sites (see Table 3). If the water is not eliminated before the optical calculation, the MNB is nearly doubled (34 %), whereas the correlation remains unchanged.

In summary, for the base case R1, while the modelled BC mass concentration is too low (by a factor of 2), the modelled particle light absorption coefficient can still match the observations with even a positive bias of about 20 %. Calculating the quotient of both, the dry α_{BC} at 637 nm can be derived. This can be then compared to α_{Csoot} from measurements. In Fig. 3c the time series of daily averaged α_{BC} for the R1 model run and the measurements of α_{Csoot} are shown. As determined from measurements, α_{Csoot} shows only little variation during this time period with values between 3 and $6\,m^2\,g^{-1}$, which is on the same level at all observation sites ranging from urban to mountain characteristics. When looking at the model values a similar behaviour can be seen. It has to be pointed out that α_{BC} is higher with values around 9 and $12\,m^2\,g^{-1}$. The overall MNB is 111 %, which is equivalent to a mean bias of $5.34\,m^2\,g^{-1}$. Regarding humidified particles,

MNB is even higher (133 %) (see Table 3). This means that in terms of simulating aerosol light absorption, the model error in the simulation of m_{BC} is somehow overcompensated by a too large α_{BC}.

3.2.2 Adjustment of the BC mass absorption cross-section

The particle light absorption coefficient is a complex function depending on the particle number size distribution, the refractive index and the mixing state of BC. While the particle number size distributions and particle mass concentrations are relatively easy to adjust, the treatment of the mixing state is a rather difficult task. An evaluation would also be difficult, because the mixing state of BC can only be directly measured by single particle analysis such as electron microscopy (Hasegawa and Ohta, 2002; Naoe et al., 2009), or the SP2 instrument (Naoe et al., 2009; Schwarz et al., 2006) or indirectly by using VTDMA measurements (Wehner et al., 2009; Cheng et al., 2009). In many models, the change of BC from hydrophobic to hydrophilic is simply parameterized by applying a fixed ageing time (Koch et al., 2009). In the version of WRF-Chem applied in this study, BC is assumed to be internally mixed with all other chemical compounds, which implies an impact on the light absorption properties of these particles by a factor up to 2-3, which may lead to the overestimation in aerosol mass absorption cross-section. To change the mixing state treatment itself in WRF-Chem is very difficult. This is because the core-shell coated treatment in the optical calculation module of WRF-Chem may result in a smaller mass absorption cross-section, but the model turns out to be non-robust and crashes during the model simulation. The treatment of external mixture of BC is inherently limited by the MOSAIC-bin model treatment of aerosol compositions; that is, there are no explicit different bins for different aerosol compositions.

So, in this study, we chose a compromise by adjusting the imaginary part of the BC refractive index so that the modelled mass absorption cross-section can match the measurements available for the simulation period from Nordmann et al. (2013). It has to be emphasized that α_{BC} is not constant and may vary during the simulation period, because Mie theory is applied in the model as described in Sect. 2.2.1.

For the adjustment procedure, the particle mass concentrations of all simulated chemical constituents are read in from the model output. Using bilinear interpolation, the model particle mass concentrations are calculated for five observation sites. Passing the interpolated particle mass concentrations of all chemical constituents to the subroutine "optical_prep_sectional.F", particle diameters and corresponding refractive indices are derived, which in turn are passed to the Mie subroutine to calculate absorption coefficients of the modelled particle population at individual measurement sites. It is important to mention that the particle light absorption coefficients are calculated for dry particles by setting the aerosol water content to zero before passing the particle mass concentrations to "optical_prep_sectional.F", because measurements were also performed for dry aerosol. Values of α_{BC} are derived at each of the measurement locations by dividing the modelled dry absorption coefficients by the modelled BC mass concentrations. This procedure can be summarized by the following scheme:

1. Obtain particle mass concentrations from the full model run.
2. Interpolate particle mass concentrations to measurement site coordinates.
3. Set aerosol water to 0.
4. Calculate volume equivalent particle diameter and refractive index in subroutine "optical_prep_sectional.F".
5. Calculate aerosol particle optical properties in the subroutine "mieaer".
6. Calculate the mass absorption cross-section (α_{BC}) from model output.

The overall deviation between measured and modelled mass absorption cross-sections is minimized in terms of the root mean square deviation (χ^2) by using a Newton–Raphson method (Press et al., 1986). For this approach, the imaginary part of the complex refractive index of BC is chosen to be the independent variable. Repeating steps 4–6 several times with modified refractive index, a new imaginary part of the complex refractive index can be found iteratively. The new imaginary part was used in WRF-Chem by modifying the default value in "optical_prep_sectional.F".

3.2.3 Particle light absorption coefficient and implication for the mixing state

In Table 5 it can be seen that the adjustment of the modified BC imaginary part leads to a slight decrease of modelled absorption coefficients at all seven sites under consideration. Especially for R3, the overall MNB is improved with a value of -2 %. The overall pattern remains almost the same since the correlation coefficient only slightly increased to 0.22 for R2 and 0.20 for R3 and R4, respectively.

The simulation of the absorption coefficient could be improved by the adjustment of α_{BC} to observed α_{Csoot} by varying the imaginary part of the BC refractive index. From the procedure described in Sect. 3.2.2, an average value of 0.263 with a standard deviation of 0.02 was found, which is much smaller than the default value in WRF-Chem of 0.71 and also the summarized range of imaginary part of BC refractive index in the literature (Bond and Bergstrom, 2006). An explanation for this result is given by Fig. 8. Theoretical values of the mass absorption cross-section were derived using the Mie code for spherical particles (Bohren and Huffman,

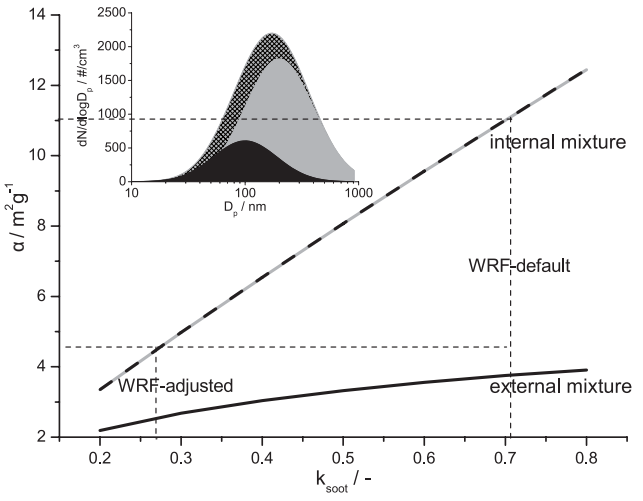

Figure 8. Mass absorption cross-section for externally and internally mixed BC particles in dependence on the imaginary part (k) of the refractive index ($m = n + ik$) from Mie calculations. Values are derived using spherical log normally distributed BC particles ($N = 800$, $Dp_g = 120\,\text{nm}$, $\sigma_g = 1.9$, $\rho = 1.8\,\text{g cm}^{-3}$, $m = 1.85 + ik$) and non-absorbing particles ($N = 2500$, $Dp_g = 200\,\text{nm}$, σ_g=2, $m = 1.55 + i1 \times 10^{-7}$)

1983) and the volume-averaging method, which is also applied in WRF-Chem. For simplicity, aerosol particles are assumed to be decomposed of an absorbing (BC) and a non-absorbing fraction. For internally mixed particles, the mass absorption cross-section was around $4.4\,\text{m}^2\,\text{g}^{-1}$ for the adjusted imaginary part of 0.263, which is in the size range of the measurements and the values in R2, R3 and R4. Repeating the calculation for the internally mixed case with the default imaginary part a mass absorption cross-section of 10.7 $\text{m}^2\,\text{g}^{-1}$ is calculated, which is in the range of the values for R1. Assuming further that all BC particles are externally mixed and taking the default imaginary part, the mass absorption cross-section is $3.6\,\text{m}^2\,\text{g}^{-1}$, which is close to the value for internal mixture and refractive index of 0.263. Assuming an externally mixed fraction of 90 % and the default imaginary part, the mass absorption cross-section is in the size range of the measurements. This strongly suggests that the discrepancy between modelled and measured mass absorption cross-section is due to the fact that a large portion of externally mixed BC is not considered in WRF-Chem. This can be compensated by lowering the imaginary part of BC refractive index from adjustment in the present study.

3.2.4 Effect on radiative forcing

The effect of BC on the radiation balance over Germany at the surface and at TOA was examined by comparing the net irradiances from R3 and an additional unperturbed model run R5 with no anthropogenic and natural EC emissions. The radiative forcing can be calculated by subtracting the radiant fluxes of the model runs with and without emissions on either the surface or at the top of the atmosphere. These calculations were performed for R3, by using the default and adjusted imaginary part of the BC refractive index. This was done in order to estimate the effect of the adjusted particle light absorption on the radiative forcing.

For the evaluation of the direct radiative forcing, grid cells containing cloud ice or water were not considered. A relatively short time period was identified, which was characterized by cloud-free conditions. The radiative forcing at the surface and at TOA for 3 April 2009 at 12:00 in the nested model domain is shown in Fig. 9 for both model runs. In general, the BC radiative forcing is negative at the surface and positive at TOA. The absolute value is higher at the surface than at TOA, which is in agreement with previous studies (Haywood and Shine, 1997; Ramanathan and Carmichael, 2008). For run R3, it can be seen that the BC radiative forcing at the surface is mostly between -2 and $-10\,\text{W m}^{-2}$ in large parts of the model domain. For the same BC concentrations, the radiative forcing at the surface using the default imaginary part of BC refractive index is higher with values between -4 and $-16\,\text{W m}^{-2}$. In some grid cells the values may be even higher especially when large point sources are situated in immediate vicinity as can be seen for example in combination with Fig. 2 in the northwestern part of the Czech Republic.

The radiative forcing for R3 at TOA is comparably small with values mostly between 0 and $4\,\text{W m}^{-2}$. Using the default BC refractive index, values between 2 and $6\,\text{W m}^{-2}$ were determined. Calculating the quotient between the radiative forcing for the runs with modified and unmodified imaginary part of the BC refractive index it was found that the decrease in radiative forcing at TOA and the surface is mostly between 30 % and 70 %.

The dependence of the radiative forcing on the vertical profile of the simulated BC mass concentration is shown in Fig. S3. It can be seen that the radiative forcing increases with higher concentration near the surface in the morning hours. In the afternoon the concentration near the surface decreases because more particles are transported to higher altitudes. This leads to a second maximum. Accordingly, model validation of the vertical profile of BC is expected to provide more information on the evaluation of BC warming effects in the future.

4 Conclusions

The main goals of the present study are the BC source and light absorption evaluations by using the regional model WRF-Chem and comprehensive field measurements over central Europe, especially over Germany. WRF-Chem was used in combination with a high-resolution EC emission inventory. Simulated BC mass concentrations were lower by around 50 %. The largest bias was found when air masses

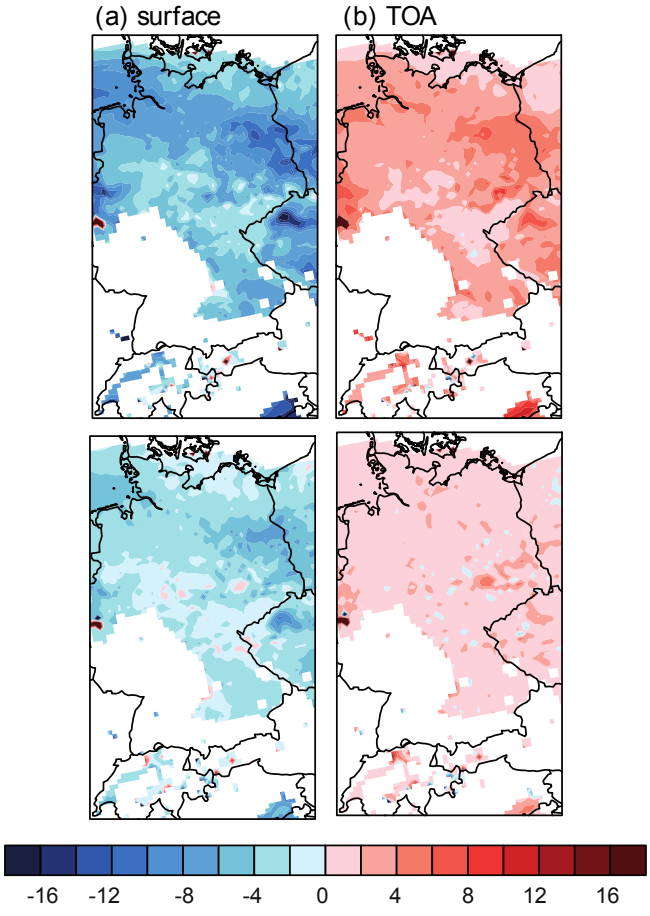

Figure 9. Direct radiative forcing in W m^{-2} for 3 April 2009 12:00 of BC at **(a)** the surface and **(b)** the top of the atmosphere, derived from the comparison of the runs with and without EC emissions. In **(a)** and **(b)** the upper panels refer to the run R3 using the unmodified imaginary part of BC in each case, whereas for the lower panels the adjusted value of 0.26 was used.

approached the observation sites from eastern directions. Additional model evaluation regarding aerosol optical depth and PM_{10} mass concentration showed a negative bias but only in the eastern and southeastern part of the domain, also suggesting that emissions might be underestimated. Three additional model runs were performed in order to improve the simulation of BC by modifying the emissions. In the first instance, the EUCAARI EC emissions were scaled to ARCTAS emissions (R2), which lowered the overall model bias to −36 %. Subsequently, another model simulation was done with EC emissions simply multiplied by a factor of 2 (R3) in each grid cell. This led to an overall further model improvement regarding the simulation of BC, but a worse model performance during the clean marine time period with additional overestimation of BC by a factor of 2. By scaling the emissions by a factor of 5 but only to the east of 15° E (R4), it was found that the simulation of the temporal trend of BC could be improved. This indicates that the emissions in the eastern European domain are more significant than in the western domain. A more precise spatial alignment would require the application of more sophisticated inverse modelling techniques. Moreover, scaling the EC emissions by a factor of 5 would have dramatic consequences for total PM_{10} and $PM_{2.5}$ emissions as EC is a fraction of PM. EC emissions are always accompanied by co-emitted other particulate matter species such as OC or mineral ashes. So, the estimated combustion related total PM emissions would also increase 3–5-fold.

Particle light absorption was evaluated using measurements of the multi-angle absorption photometer at several sites in Germany. It was found that the model slightly overestimates the absorption coefficient by 20 % even when the BC mass concentration is underestimated by a factor of 2. Accordingly, mass absorption cross-sections were hence overestimated by 111 %. The mass absorption cross-sections were adjusted to measurements, which were available for the considered time period from Nordmann et al. (2013). This was done by iteratively modifying the imaginary part of the BC refractive index. This leads to a rather constant but very low value of 0.263, which could be attributed to the mixing state of BC particles. The mass absorption cross-sections determined by Nordmann et al. (2013) showed only little variation in time and for different observation sites, indicating only small variations in the mixing state. Applying a simple Mie model for mixed spherical particles it was found that the absolute value of the mass absorption cross-section could be theoretically explained if the majority of BC particles would be externally mixed.

The radiative forcing of BC particles was calculated for the default settings of the optical module and for the adjusted version using the calculated imaginary part. The most important finding was that the optical adjustment leads to a decrease in BC direct radiative forcing of BC particles at TOA and at the surface between 30 % and 70 %. As a consequence, for estimating the direct radiative forcing of BC particles it is crucial to take the BC mixing state into account in the calculation of the particle light absorption coefficient. Because this is generally difficult to realize, at least the mass absorption cross-section has to be set correctly.

The Supplement related to this article is available online at doi:10.5194/acp-14-12683-2014-supplement.

Acknowledgements. This work was supported by the German Federal Ministry for the Environment, Nature Conservation and Nuclear Safety (BMU) grants F& E 370343200 (German title: "Erfassung der Zahl feiner und ultrafeiner Partikel in der Aussenluft") and F& E 371143232 (German title: "Trendanalysen gesundheitsgefährdender Fein- und Ultrafeinstaubfraktionen unter Nutzung der im German Ultrafine Aerosol Network (GUAN) ermittelten Immissionsdaten durch Fortführung und Interpretation der Messreihen"). S. Nordmann acknowledges support by a personal scholarship of the Deutsche Bundesstiftung Umwelt (DBU). We acknowledge the German federal environmental agency for kindly providing the PM_{10} data from their measurement network. We also recognize that this work was supported in part by the USEPA STAR grant # RD-83503701 and by the European Commission under the projects PEGASOS (grant no. 265148).

The service charges for this open access publication have been covered by the Max Planck Society.

Edited by: Y. Balkanski

References

Ackerman, A., Toon, O., Stevens, D., Heymsfield, A., Ramanathan, V., and Welton, E.: Reduction of Tropical Cloudiness by Soot, Science, 288, 1042–1047, 2000.

Andreae, M. and Gelencser, A.: Black carbon or brown carbon? The nature of light-absorbing carbonaceous aerosols, Atmos. Chem. Phys., 6, 3131–3148, 2006, http://www.atmos-chem-phys.net/6/3131/2006/.

Barnard, J. C., Fast, J. D., Paredes-Miranda, G., Arnott, W. P., and Laskin, A.: Technical Note: Evaluation of the WRF-Chem "Aerosol Chemical to Aerosol Optical Properties" Module using data from the MILAGRO campaign, Atmos. Chem. Phys., 10, 7325–7340, doi:10.5194/acp-10-7325-2010, 201.

Birmili, W., Weinhold, K., Nordmann, S., Wiedensohler, A., Spindler, G., Müller, K., Herrmann, H., Gnauk, T., Pitz, M., Cyrys, J., Flentje, H., Nickel, C., Kuhlbusch, T., Löschau, G., Haase, D., Meinhardt, F., Schwerin, A., Ries, L., and Wirtz, K.: Atmospheric aerosol measurements in the German Ultrafine Aerosol Network (GUAN) – Part – Soot and Particle Number Size Distributions, Gefahrst. Reinh. Luft, 69, 137–145, 2009.

Bohren, C. and Huffman, D.: Absorption and scattering of light by small particles, Wiley Online Library, New York, 1983.

Bond, T. and Bergstrom, R.: Light absorption by carbonaceous particles: An investigative review, Aerosol Sci. Tech., 40, 27–67, 2006.

Bond, T. C., Bhardwaj, E., Dong, R., Jogani, R., Jung, S., Roden, C., Streets, D. G., and Trautmann, N. M.: Historical emissions of black and organic carbon aerosol from energy-related combustion, 1850-2000, Global Biogeochem. Cy., 21, GB2018, doi:10.1029/2006GB002840, 2007.

Chapman, E., Gustafson Jr., W., Easter, R., Barnard, J., Ghan, S., Pekour, M., and Fast, J.: Coupling aerosol-cloud-radiative processes in the WRF-Chem model: Investigating the radiative impact of elevated point sources, Atmos. Chem. Phys., 9, 945–964, 2009, http://www.atmos-chem-phys.net/9/945/2009/.

Cheng, Y. F., Berghof, M., Garland, R. M., Wiedensohler, A., Wehner, B., Müller, T., Su, H., Zhang, Y. H., Achtert, P., Nowak, A., Pöschl, U., Zhu, T., Hu, M., and Zeng, L. M.: Influence of soot mixing state on aerosol light absorption and single scattering albedo during air mass aging at a polluted regional site in northeastern China, J. Geophys. Res.-Atmos., 114, D00G10, doi:10.1029/2008JD010883, 2009.

Chi, X., Winderlich, J., Mayer, J.-C., Panov, A. V., Heimann, M., Birmili, W., Heintzenberg, J., Cheng, Y., and Andreae, M. O.: Long-term measurements of aerosol and carbon monoxide at the ZOTTO tall tower to characterize polluted and pristine air in the Siberian taiga, Atmos. Chem. Phys., 13, 12271–12298, doi:10.5194/acp-13-12271-2013, 2013.

Chou, M., Suarez, M., Ho, C., Yan, M., and Lee, K.: Parameterizations for Cloud Overlapping and Shortwave Single-Scattering Properties for Use in General Circulation and Cloud Ensemble Models, J. Climate, 11, 202–214, 1998.

Darmenov, A. and da Silva, A.: The Quick Fire Emissions Dataset (QFED) - Documentation of versions 2.1, 2.2 and 2.4. NASA Technical Report Series on Global Modeling and Data Assimilation., Report, NASA TM-2013-104606, Goddard Space Flight Center Greenbelt MD, 2013.

Fast, J., Gustafson Jr, W., Easter, R., Zaveri, R., Barnard, J., Chapman, E., Grell, G., and Peckham, S.: Evolution of ozone, particulates, and aerosol direct radiative forcing in the vicinity of Houston using a fully coupled meteorology-chemistry-aerosol model, J. Geophys. Res., 111, D21305, doi:10.1029/2005JD006721, 2006.

Fuller, K. A., Malm, W. C., and Kreidenweis, S. M.: Effects of mixing on extinction by carbonaceous particles, J. Geophys. Res.-Atmos., 104, 15941–15954, doi:10.1029/1998JD100069, 1999.

Genberg, J., Denier van der Gon, H. A. C., Simpson, D., Swietlicki, E., Areskoug, H., Beddows, D., Ceburnis, D., Fiebig, M., Hansson, H. C., Harrison, R. M., Jennings, S. G., Saarikoski, S., Spindler, G., Visschedijk, A. J. H., Wiedensohler, A., Yttri, K. E., and Bergström, R.: Light-absorbing carbon in Europe – measurement and modelling, with a focus on residential wood combustion emissions, Atmos. Chem. Phys., 13, 8719–8738, doi:10.5194/acp-13-8719-2013, 2013.

Ghan, S., Laulainen, N., Easter, R., Wagener, R., Nemesure, S., Chapman, E., Zhang, Y., and Leung, R.: Evaluation of aerosol direct radiative forcing in MIRAGE, J. Geophys. Res., 106, 5295–5316, 2001.

Grell, G., Peckham, S., Schmitz, R., McKeen, S., Frost, G., Skamarock, W., and Eder, B.: Fully coupled "online" chemistry within the WRF model, Atmos. Environ., 39, 6957–6975, 2005.

Guenther, A., Karl, T., Harley, P., Wiedinmyer, C., Palmer, P. I., and Geron, C.: Estimates of global terrestrial isoprene emissions using MEGAN (Model of Emissions of Gases and Aerosols from Nature), Atmos. Chem. Phys., 6, 3181–3210, doi:10.5194/acp-6-3181-2006, 2006.

Hasegawa, S. and Ohta, S.: Some measurements of the mixing state of soot-containing particles at urban and non-urban sites, Atmos. Environ., 36, 3899–3908, 2002.

Haywood, J. and Shine, K.: Multi-spectral calculations of the direct radiative forcing of tropospheric sulphate and soot aerosols using a column model, Q. J. Roy. Meteor. Soc., 123, 1907–1930, 1997.

Holben, B., Eck, T., Slutsker, I., Tanre, D., Buis, J., Setzer, A., Vermote, E., Reagan, J., Kaufman, Y., Nakajima, T., Lavenu, F.,

Jankowiak, I., and Smirnov, A.: AERONET-A Federated Instrument Network and Data Archive for Aerosol Characterization, Remote Sens. Environ., 66, 1–16, 1998.

Hyer, E. J., Reid, J. S., and Zhang, J.: An over-land aerosol optical depth data set for data assimilation by filtering, correction, and aggregation of MODIS Collection 5 optical depth retrievals, Atmospheric Measurement Techniques, 4, 379–408, doi:10.5194/amt-4-379-2011, 2011.

IPCC: Climate Change 2013: The Physical Science Basis. Contribution of Working Group I to the Fifth Assessment Report of the Intergovernmental Panel on Climate Change, Report, Cambridge University Press, New York, 2013.

Janjic, Z.: The Step-Mountain Eta Coordinate Model: Further Developments of the Convection, Viscous Sublayer, and Turbulence Closure Schemes, Mon. Weather Rev., 122, 927–945, 1994.

Junker, C. and Liousse, C.: A global emission inventory of carbonaceous aerosol from historic records of fossil fuel and biofuel consumption for the period 1860–1997, Atmos. Chem. Phys., 8, 1195–1207, doi:10.5194/acp-8-1195-2008, 2008.

Khalizov, A., Zhang, R., Zhang, D., Xue, H., Pagels, J., and McMurry, P.: Formation of highly hygroscopic soot aerosols upon internal mixing with sulfuric acid vapor, J. Geophys. Res., 114, D05208, doi:10.1029/2008JD010595, 2009.

Kinne, S., Schulz, M., Textor, C., Guibert, S., Balkanski, Y., Bauer, S. E., Berntsen, T., Berglen, T. F., Boucher, O., Chin, M., Collins, W., Dentener, F., Diehl, T., Easter, R., Feichter, J., Fillmore, D., Ghan, S., Ginoux, P., Gong, S., Grini, A., Hendricks, J., Herzog, M., Horowitz, L., Isaksen, I., Iversen, T., Kirkevåg, A., Kloster, S., Koch, D., Kristjansson, J. E., Krol, M., Lauer, A., Lamarque, J. F., Lesins, G., Liu, X., Lohmann, U., Montanaro, V., Myhre, G., Penner, J., Pitari, G., Reddy, S., Seland, O., Stier, P., Takemura, T., and Tie, X.: An AeroCom initial assessment - optical properties in aerosol component modules of global models, Atmos. Chem. Phys., 6, 1815–1834, doi:10.5194/acp-6-1815-2006, 2006.

Koch, D. and Del Genio, A. D.: Black carbon semi-direct effects on cloud cover: review and synthesis, Atmos. Chem. Phys., 10, 7685–7696, 2010, http://www.atmos-chem-phys.net/10/7685/2010/.

Koch, D., Schulz, M., Kinne, S., McNaughton, C., Spackman, J. R., Balkanski, Y., Bauer, S., Berntsen, T., Bond, T. C., Boucher, O., Chin, M., Clarke, A., De Luca, N., Dentener, F., Diehl, T., Dubovik, O., Easter, R., Fahey, D. W., Feichter, J., Fillmore, D., Freitag, S., Ghan, S., Ginoux, P., Gong, S., Horowitz, L., Iversen, T., Kirkevåg, A., Klimont, Z., Kondo, Y., Krol, M., Liu, X., Miller, R., Montanaro, V., Moteki, N., Myhre, G., Penner, J. E., Perlwitz, J., Pitari, G., Reddy, S., Sahu, L., Sakamoto, H., Schuster, G., Schwarz, J. P., Seland, Ø., Stier, P., Takegawa, N., Takemura, T., Textor, C., van Aardenne, J. A., and Zhao, Y.: Evaluation of black carbon estimations in global aerosol models, Atmos. Chem. Phys., 9, 9001–9026, doi:10.5194/acp-9-9001-2009, 2009.

Kulmala, M., Asmi, A., Lappalainen, H. K., Baltensperger, U., Brenguier, J.-L., Facchini, M. C., Hansson, H.-C., Hov, Ø., O'Dowd, C. D., Pöschl, U., Wiedensohler, A., Boers, R., Boucher, O., de Leeuw, G., Denier van der Gon, H. A. C., Feichter, J., Krejci, R., Laj, P., Lihavainen, H., Lohmann, U., McFiggans, G., Mentel, T., Pilinis, C., Riipinen, I., Schulz, M., Stohl, A., Swietlicki, E., Vignati, E., Alves, C., Amann, M., Ammann, M., Arabas, S., Artaxo, P., Baars, H., Beddows, D. C. S., Bergström, R., Beukes, J. P., Bilde, M., Burkhart, J. F., Canonaco, F., Clegg, S. L., Coe, H., Crumeyrolle, S., D'Anna, B., Decesari, S., Gilardoni, S., Fischer, M., Fjaeraa, A. M., Fountoukis, C., George, C., Gomes, L., Halloran, P., Hamburger, T., Harrison, R. M., Herrmann, H., Hoffmann, T., Hoose, C., Hu, M., Hyvärinen, A., Hõrrak, U., Iinuma, Y., Iversen, T., Josipovic, M., Kanakidou, M., Kiendler-Scharr, A., Kirkevåg, A., Kiss, G., Klimont, Z., Kolmonen, P., Komppula, M., Kristjánsson, J.-E., Laakso, L., Laaksonen, A., Labonnote, L., Lanz, V. A., Lehtinen, K. E. J., Rizzo, L. V., Makkonen, R., Manninen, H. E., McMeeking, G., Merikanto, J., Minikin, A., Mirme, S., Morgan, W. T., Nemitz, E., O'Donnell, D., Panwar, T. S., Pawlowska, H., Petzold, A., Pienaar, J. J., Pio, C., Plass-Duelmer, C., Prévôt, A. S. H., Pryor, S., Reddington, C. L., Roberts, G., Rosenfeld, D., Schwarz, J., Seland, Ø., Sellegri, K., Shen, X. J., Shiraiwa, M., Siebert, H., Sierau, B., Simpson, D., Sun, J. Y., Topping, D., Tunved, P., Vaattovaara, P., Vakkari, V., Veefkind, J. P., Visschedijk, A., Vuollekoski, H., Vuolo, R., Wehner, B., Wildt, J., Woodward, S., Worsnop, D. R., van Zadelhoff, G.-J., Zardini, A. A., Zhang, K., van Zyl, P. G., Kerminen, V.-M., S Carslaw, K., and Pandis, S. N.: General overview: European Integrated project on Aerosol Cloud Climate and Air Quality interactions (EUCAARI) – integrating aerosol research from nano to global scales, Atmos. Chem. Phys., 11, 13061–13143, doi:10.5194/acp-11-13061-2011, 2011.

Lamarque, J.-F., Bond, T. C., Eyring, V., Granier, C., Heil, A., Klimont, Z., Lee, D., Liousse, C., Mieville, A., Owen, B., Schultz, M. G., Shindell, D., Smith, S. J., Stehfest, E., Van Aardenne, J., Cooper, O. R., Kainuma, M., Mahowald, N., McConnell, J. R., Naik, V., Riahi, K., and van Vuuren, D. P.: Historical (1850-2000) gridded anthropogenic and biomass burning emissions of reactive gases and aerosols: methodology and application, Atmos. Chem. Phys., 10, 7017–7039, doi:10.5194/acp-10-7017-2010, 2010.

Levy, R., Remer, L., Mattoo, S., Vermote, E., and Kaufman, Y.: Second-generation operational algorithm: Retrieval of aerosol properties over land from inversion of Moderate Resolution Imaging Spectroradiometer spectral reflectance, J. Geophys. Res., 112, D13211, doi:10.1029/2006JD007811, 2007.

Lin, Y., Farley, R., and Orville, H.: Bulk Parameterization of the Snow Field in a Cloud Model, J. Clim. Appl.Meteorol., 22, 1065–1092, 1983.

Mikhailov, E. F., Vlasenko, S. S., Podgorny, I. A., Ramanathan, V., and Corrigan, C. E.: Optical properties of soot–water drop agglomerates: An experimental study, J. Geophys. Res.-Atmos., 111, 2156–2202, doi:10.1029/2005JD006389, 2006.

Müller, T., Henzing, J. S., de Leeuw, G., Wiedensohler, A., Alastuey, A., Angelov, H., Bizjak, M., Collaud Coen, M., Engström, J. E., Gruening, C., Hillamo, R., Hoffer, A., Imre, K., Ivanow, P., Jennings, G., Sun, J. Y., Kalivitis, N., Karlsson, H., Komppula, M., Laj, P., Li, S.-M., Lunder, C., Marinoni, A., Martins dos Santos, S., Moerman, M., Nowak, A., Ogren, J. A., Petzold, A., Pichon, J. M., Rodriquez, S., Sharma, S., Sheridan, P. J., Teinilä, K., Tuch, T., Viana, M., Virkkula, A., Weingartner, E., Wilhelm, R., and Wang, Y. Q.: Characterization and intercomparison of aerosol absorption photometers: result of two intercomparison workshops, Atmospheric Measurement Techniques, 4, 245–268, doi:10.5194/amt-4-245-2011, 2011.

Naoe, H., Hasegawa, S., Heintzenberg, J., Okada, K., Uchiyama, A., Zaizen, Y., Kobayashi, E., and Yamazaki, A.: State of mixture of atmospheric submicrometer black carbon particles and its effect on particulate light absorption, Atmos. Environ., 43, 1296–1301, 2009.

Nessler, R., Weingartner, E., and Baltensperger, U.: Effect of humidity on aerosol light absorption and its implications for extinction and the single scattering albedo illustrated for a site in the lower free troposphere, J. Aerosol Sci., 36, 958–972, doi:http://dx.doi.org/10.1016/j.jaerosci.2004.11.012, 2005.

Nordmann, S., Birmili, W., Weinhold, K., Müller, K., Spindler, G., and Wiedensohler, A.: Measurements of the mass absorption cross section of atmospheric soot particles using Raman spectroscopy, J. Geophys. Res.-Atmos., 118, 12,075–12,085, doi:10.1002/2013JD020021, 2013.

Petzold, A. and Schönlinner, M.: Multi-angle absorption photometry-a new method for the measurement of aerosol light absorption and atmospheric black carbon, J. Aerosol Sci., 35, 421–441, 2004.

Petzold, A., Ogren, J., Fiebig, M., Laj, P., Li, S.-M., Baltensperger, U., Holzer-Popp, T., Kinne, S., Pappalardo, G., Sugimoto, N., Wehrli, C., Wiedensohler, A., and Zhang, X.-Y.: Recommendations for reporting" black carbon" measurements, Atmos. Chem. Phys., 13, 8365–8379, 2013, http://www.atmos-chem-phys.net/13/8365/2013/.

Press, W., Flanner, B., Teukolsky, S., and Vetterling, W.: Numerical recipes, vol. 547, Cambridge University Press, New York, 1986.

Ramanathan, V. and Carmichael, G.: Global and regional climate changes due to black carbon, Nature Geosci, 1, 221–227, doi:10.1038/ngeo156, 2008.

Remer, L. A., Kaufman, Y. J., Tanré, D., Mattoo, S., Chu, D. A., Martins, J. V., Li, R.-R., Ichoku, C., Levy, R. C., Kleidman, R. G., Eck, T. F., Vermote, E., and Holben, B. N.: The MODIS Aerosol Algorithm, Products, and Validation., J. Aerosol Sci., 62, 947–973, 2005.

Rose, D., Wehner, B., Ketzel, M., Engler, C., Voigtländer, J., Tuch, T., and Wiedensohler, A.: Atmospheric number size distributions of soot particles and estimation of emission factors, Atmos. Chem. Phys., 6, 1021–1031, 2006, http://www.atmos-chem-phys.net/6/1021/2006/.

Rose, D., Gunthe, S. S., Su, H., Garland, R. M., Yang, H., Berghof, M., Cheng, Y. F., Wehner, B., Achtert, P., Nowak, A., Wiedensohler, A., Takegawa, N., Kondo, Y., Hu, M., Zhang, Y., Andreae, M. O., and Pöschl, U.: Cloud condensation nuclei in polluted air and biomass burning smoke near the mega-city Guangzhou, China - Part 2: Size-resolved aerosol chemical composition, diurnal cycles, and externally mixed weakly CCN-active soot particles, Atmos. Chem. Phys., 11, 2817–2836, doi:10.5194/acp-11-2817-2011, 2011.

Schaap, M., Timmermans, R., Koelemeijer, R., de Leeuw, G., and Builtjes, P.: Evaluation of MODIS aerosol optical thickness over Europe using sun photometer observations, Atmos. Environ., 42, 2187–2197, 2008.

Schwarz, J. P., Gao, R. S., Fahey, D. W., Thomson, D. S., Watts, L. A., Wilson, J. C., Reeves, J. M., Darbeheshti, M., Baumgardner, D. G., Kok, G. L., Chung, S. H., Schulz, M., Hendricks, J., Lauer, A., Kärcher, B., Slowik, J. G., Rosenlof, K. H., Thompson, T. L., Langford, A. O., Loewenstein, M., and Aikin, K. C.: Single-particle measurements of midlatitude black carbon and light-scattering aerosols from the boundary layer to the lower stratosphere, J. Geophys. Res.-Atmos., 111, 2156–2202, doi:10.1029/2006JD007076, 2006.

Sheridan, P. J., Arnott, W. P., Ogren, J. A., Andrews, E., Schmid, B., Strawa, A. W., Varma, R., and Virkkula, A.: The Reno Aerosol Optics Study: An Evaluation of Aerosol Absorption Measurement Methods, Aerosol Sci. Tech., 39, 1–16, 2005.

Skamarok, W., Klemp, J., Dudhia, J., Gill, D., Barker, D., Duda, M., Huang, X.-Y., Wang, W., and Powers, J.: A Description of the Advanced Research WRF Version 3, Report, National Center for Atmospheric Research, Boulder, Colorado, 2008.

Spracklen, D. V., Carslaw, K. S., Pöschl, U., Rap, A., and Forster, P. M.: Global cloud condensation nuclei influenced by carbonaceous combustion aerosol, Atmos. Chem. Phys., 11, 9067–9087, doi:10.5194/acp-11-9067-2011, 2011.

Vignati, E., Karl, M., Krol, M., Wilson, J., Stier, P., and Cavalli, F.: Sources of uncertainties in modelling black carbon at the global scale, Atmos. Chem. Phys., 10, 2595–2611, doi:10.5194/acp-10-2595-2010, 2010.

Visschedijk, A. and Denier van der Gon, H.: EUCAARI deliverable D42: Pan-European Carbonaceous aerosol inventory, Report, TNO Built Environment and Geosciences, Utrecht, Netherlands, 2008.

Wehner, B., Berghof, M., Cheng, Y., Achtert, P., Birmili, W., Nowak, A., Wiedensohler, A., Garland, R., Pö, schl, U., Hu, M., and Zhu, T.: Mixing state of nonvolatile aerosol particle fractions and comparison with light absorption in the polluted Beijing region, J. Geophys. Res., 114, D00G17, doi:10.1029/2008JD010923, 2009.

Weingartner, E., Burtscher, H., and Baltensperger, U.: Hygroscopic properties of carbon and diesel soot particles, Atmos. Environ., 31, 2311–2327, 1997.

Wiedinmyer, C., Akagi, S. K., Yokelson, R. J., Emmons, L. K., Al-Saadi, J. A., Orlando, J. J., and Soja, A. J.: The Fire INventory from NCAR (FINN): a high resolution global model to estimate the emissions from open burning, Geoscientific Model Development, 4, 625–641, doi:10.5194/gmd-4-625-2011, http://www.geosci-model-dev.net/4/625/2011/, 2011.

Zaveri, R., Easter, R., Fast, J., and Peters, L.: Model for simulating aerosol interactions and chemistry (MOSAIC), J. Geophys. Res., 113, D13204, doi:10.1029/2007JD008782, 2008.

Zhang, Y., Sartelet, K., Wu, S.-Y., and Seigneur, C.: Application of WRF/Chem-MADRID and WRF/Polyphemus in Europe-Part 1: Model description, evaluation of meteorological predictions, and aerosol-meteorology interactions, Atmos. Chem. Phys., 13, 6807–6843, doi:10.5194/acp-13-6807-2013, 2013.